# Stacking versatility in alkali-mixed Honeycomb Layered NaKNi2TeO6

Romain Berthelot, Jon Serrano-Sevillano, Bernard Fraisse, François Fauth, François Weill, Danielle Laurencin, Montse Casas-Cabanas, Dany Carlier, Gwenaëlle Rousse, Marie-Liesse Doublet

**Stacking versatility in alkali-mixed honeycomb layered $NaKNi_2TeO_6$**

Romain Berthelot,[1,2,*] Jon Serrano-Sevillano,[3,4,5] Bernard Fraisse,[1] François Fauth,[6] François Weill,[4] Danielle Laurencin,[1] Montse Casas-Cabanas,[3,5,7] Dany Carlier,[2,4,5] Gwenaëlle Rousse,[2,8,9] Marie-Liesse Doublet[1,2]

1 : ICGM, Univ Montpellier, CNRS, ENSCM, Montpellier, France

2 : Réseau sur le Stockage Électrochimique de l'Énergie (RS2E), CNRS, Amiens, France

3 : CIC energiGUNE, Parque Tecnológico de Álava, C/Albert Einstein 48, 01510 Miñano, Álava Spain

4 : CNRS, Bordeaux INP, ICMCB UMR5026, Université Bordeaux, F-33600 Pessac France

5 : Alistore-European Research Institute, CNRS, Amiens, 80000, France

6 : CELLS – ALBA Synchrotron 08290 Cerdanyola del Vallès, Barcelona, Spain

7 : IKERBASQUE, Basque Foundation for Science, María Díaz de Haro 3, 48013, Bilbao, Spain.

8 : Chimie du Solide et Energie, UMR8260, Collège de France, 11 place Marcelin Berthelot, 75231 Paris, France

9 : Sorbonne Université, 4 place Jussieu, F-75005 Paris, France

**Corresponding author:**

Dr. Romain Berthelot: romain.berthelot@umontpellier.fr

Institut Charles Gerhardt de Montpellier, CC1502 – 2 place Bataillon – 34095 Montpellier, France

**Abstract**

The reaction between P2-type honeycomb layered oxides $Na_2Ni_2TeO_6$ and $K_2Ni_2TeO_6$ enables the formation of $NaKNi_2TeO_6$. The compound is characterized by X-ray diffraction and $^{23}Na$ solid-state nuclear magnetic resonance spectroscopy and the structure is discussed through density functional theory calculations. In addition to the honeycomb Ni/Te cationic ordering, $NaKNi_2TeO_6$ exhibits a unique example of alternation of sodium and potassium layers instead of a random alkali-mixed occupancy. Stacking faults simulations underline the impact of the successive position of the Ni/Te honeycomb layers and validate the presence of multiple stacking sequences within the powder material, in proportions that evolve with the synthesis conditions. In a broader context, this work participates to a better understanding of the alkali-mixed layered compounds.

**Keywords**

alkali transition metal layered oxide, honeycomb ordering, DFT, solid-state NMR, stacking faults

## Introduction

Layered alkali transition metal oxides gather a wide range of chemical compositions and various correlated physical properties. Their crystallographic structure is usually described as a stacking of edge-shared $MO_6$ octahedra layers with alkali ions being inserted in the interlayer space. Cationic substitutions within the transition metal layers are generally easy to achieve thanks to the very close ionic radii in octahedral symmetry of a wide range of elements (transition metals, and also *s*- and *p*-block elements).This chemical diversity offers a wonderful playground for chemists and physicists to design multi-metal layered oxides and to tune their electronic properties, as witnessed by the tremendous efforts devoted to studying this family of materials for electrochemical applications.[1–3] For particular substitutions leading to $A_xM_{2/3}M'_{1/3}O_2$ compositions wit M and M' being cations of different size, a honeycomb-like cationic ordering might appear within the transition metal layer, with each $M'O_6$ octahedron being surrounded by six other $MO_6$ octahedra. In this group of compositions, O3-type Li-rich layered compounds $Li_2MO_3$ ($Li[Li_{1/3}M_{2/3}]O_2$) have been brought to light for promoting anionic redox chemistry in high-capacity electrodes.[4–9] The magnetic behavior of honeycomb-ordered layered compounds is also widely investigated.[10]

In 2011, Evstigneeva and coworkers reported on the fast sodium ionic conductivity in the family of $Na_2M_2TeO_6$ – $Na_{2/3}(M_{2/3}Te_{1/3})O_2$ – compounds, with M being Ni, Co, Zn or Mg.[11] Keeping the P2-type oxygen stacking[12] and the in-plane Ni/Te honeycomb cationic ordering (Figure 1a), the structural difference between all the compositions lies on the relative position of the tellurium cations from one layer to the next (Figure 1b). For $Na_2Ni_2TeO_6$, straight chains of tellurium and nickel are observed along the hexagonal $c_{hex.}$-axis, whereas "zigzag" tellurium sequences characterize the other compositions. The latter was confirmed by the group of Cava in a parallel study focused on $Na_2Co_2TeO_6$.[13] Nickel substitutions by other metals are possible through a solid-solution behavior and induce a progressive shift from one stacking sequence to

the other.[14] In the alkali interlayer space, various trigonal prismatic sites are possible for the sodium cations depending on whether the $NaO_6$ prism shares faces with $MO_6$ and/or $TeO_6$ octahedra (Figure 1c). $Na_2Ni_2TeO_6$ was also investigated as electrode material for Na-ion battery.[15,16] Since 2018, Masese and coworkers have been investigating the potassium layered analogs $K_2M_2TeO_6$ and underlined their interesting electrochemical behavior in K-ion batteries.[17–19] The crystallographic structure of $K_2Ni_2TeO_6$ was solved using the $Na_2Ni_2TeO_6$ structural model resulting in the expected increase of the cell parameters mainly induced by the thicker alkali interlayer, and in a significant difference in the potassium cations distribution (Table S1).

In the family of alkali transition metal layered oxides, there are only few examples of alkali-mixed compositions. In 1994, Balsys and Davis reported on the $Li_xNa_yCoO_2$ phase and described its layered structure as an alternation of O3-$LiCoO_2$ and P2-$Na_xCoO_2$ blocks.[20] This unique OP4 stacking was later studied by some of us and others especially to prepare the O4-type form of $LiCoO_2$ by topotactic ionic exchange.[21–23]

Searching for other alkali-mixed compositions, in this work we investigated the solid-solid reaction between honeycomb layered oxides $Na_2Ni_2TeO_6$ and $K_2Ni_2TeO_6$. The formation of a new lamellar phase $NaKNi_2TeO_6$ is evidenced by powder diffraction techniques, coupled with $^{23}Na$ solid-state nuclear magnetic resonance spectroscopy and density functional theory calculations. The structure of $NaKNi_2TeO_6$ exhibits an alternation of sodium and potassium blocks; however, the stacking disorder does not allow solving the complete crystallographic structure. Additionally, stacking faults simulations enabled to validate the presence of multiple possible stacking sequences in the powder material.

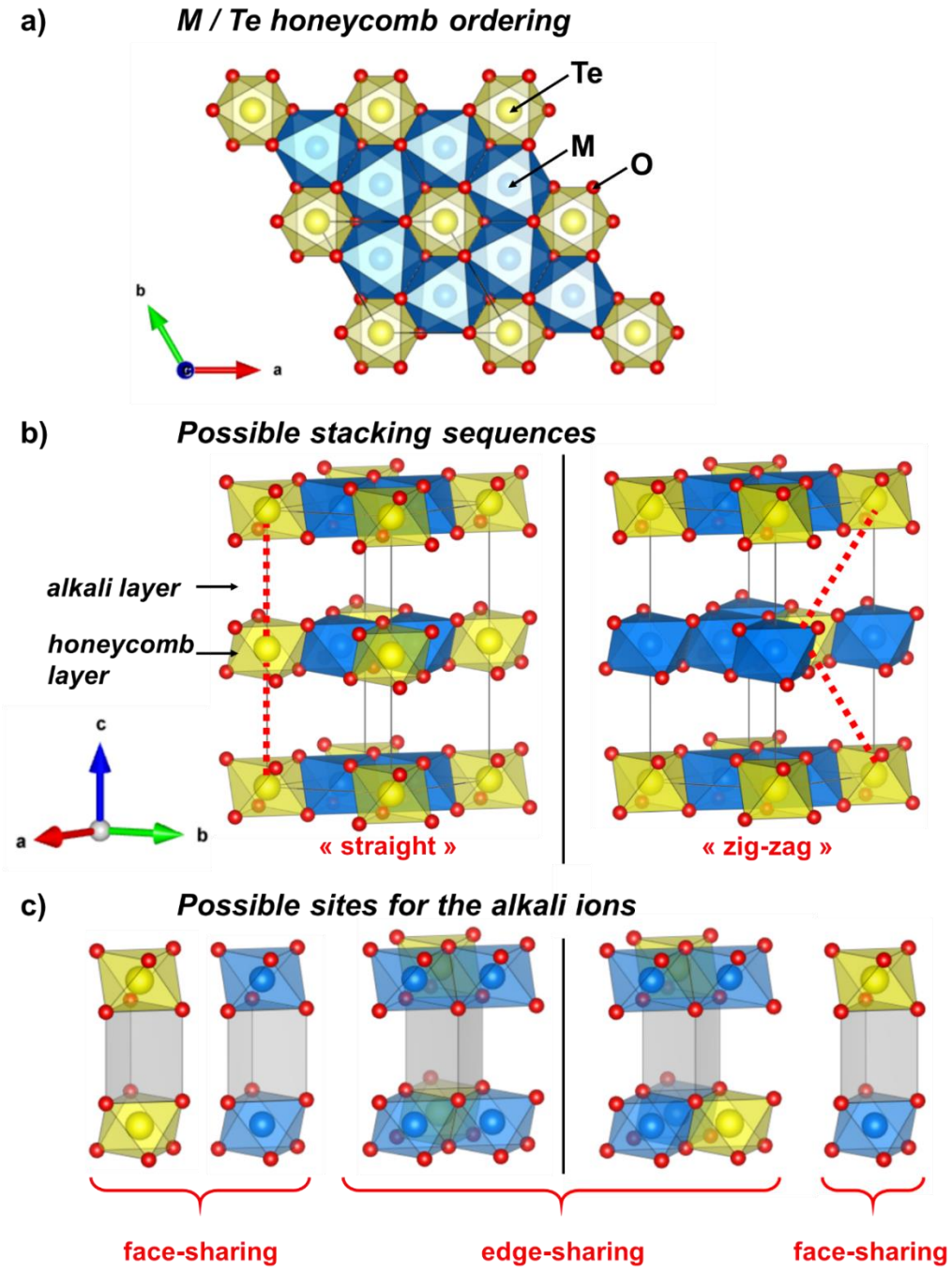


*Figure 1: Crystallographic features of P2-type $A_2M_2TeO_6$ layered compounds: (a) top view of the honeycomb cationic ordering between nickel and tellurium cations (in blue and yellow, respectively), (b) perspective view of the two possible stacking sequences according to the sequence of the tellurium cations in dashed red lines, with alkali ions omitted for clarity, (c) possible $AO_6$ trigonal prismatic sites (in grey) corresponding to each stacking, sharing faces with $MO_6$ only, $TeO_6$ only, $MO_6$ and $TeO_6$, or sharing edges. In layered $A_2M_2TeO_6$ compounds, the space groups corresponding to the straight and "zigzag" tellurium sequences are $P6_3/mcm$ and $P6_322$, respectively.*

## Experimental

$Na_2Ni_2TeO_6$ and $K_2Ni_2TeO_6$ precursors were prepared by conventional solid-state reaction, by adapting previously reported procedures.[11,14,17,18,24] Anhydrous alkali carbonates ($Na_2CO_3$, Sigma-Aldrich, ≥ 99.5 % or $K_2CO_3$, Sigma-Aldrich, ≥ 99.0 %), tellurium oxide ($TeO_2$, Alfa-Aesar, 99.99%) and nickel oxide (NiO, Alfa-Aesar, 99 %) were mixed together, pelletized and then heated in a gold crucible. A nominal 10 wt.% excess of alkali carbonates was used to balance the high-temperature loss of alkali oxides. In the literature, $Na_2Ni_2TeO_6$ and $K_2Ni_2TeO_6$ are usually prepared at 900 and 800 °C. As our attempts to prepare $K_2Ni_2TeO_6$ at 900 °C were unsuccessful, we choose to prepare the precursors at 800 °C (9 hours in air with heating rate of 2.5 °C/min). To synthetize $NaKNi_2TeO_6$, stoichiometric blends of the as-prepared precursors were then heated under five various conditions of dwell temperatures and durations (9h at 200, 400, 600 or 800 °C, and also 4 days at 800 °C. To avoid any moisture contamination, sample powders were taken out of the furnace at 150 °C on cooling and transferred to an argon-filled glovebox.

Laboratory X-ray powder diffraction (XRPD) analyses were performed with a PANalytical X'Pert θ/θ diffractometer with Cu Kα radiation in an airtight sample holder for preliminary profile matching refinement. The powder sample of $NaKNi_2TeO_6$ obtained after 9 hours at 800 °C was also analyzed by high angular resolution synchrotron X-ray powder diffraction (SXRPD) collected on BL04_MSPD beamline of the ALBA synchrotron (Cerdanyola del Vallès, Spain).[25,26] Here, the sample powder was enclosed in a 0.7 mm diameter quartz capillary sealed in argon atmosphere, and data were collected in transmission geometry at a wavelength of λ = 0.49589 Å. Profile matching refinement and Rietveld attempts were carried out using the FullProf suite.[27] Electron diffraction was performed on the same powder. Patterns were obtained using a JEOL 2100 transmission electron microscope equipped with an Orius 200D

camera from GATAN. Prior to the observation, the sample was crushed in alcohol and a drop of this suspension was deposited on a carbon-supported film on a copper grid.

$^{23}$Na solid-state nuclear magnetic resonance spectroscopy (NMR) was performed on powder samples of $Na_2Ni_2TeO_6$ and $NaKNi_2TeO_6$ using a Bruker Avance spectrometer at 79.4 MHz (7.05 T magnet). The samples are introduced in 2.5 mm zirconia rotors inside a glovebox. $^{23}$Na Magic Angle Spinning Nuclear Magnetic Resonance (MAS-NMR) experiments were carried out using a 30 kHz spinning frequency. The spectral width was set to 1 MHz, and the recycle time to $D_0$ = 0.2 s, which was long enough to avoid the *T1* saturation effects. A one rotor period synchronized Hahn echo sequence ($\pi/2$-delay- $\pi$) with a $\pi/2$ = 2 µs pulse duration was used. The center of the experimental window was set to 680 ppm, in the region of the maximum intensities observed, with 0.1 M NaCl aqueous solution as external reference. Attempts to record $^{39}$K solid-state NMR spectra on both $K_2Ni_2TeO_6$ and $NaKNi_2TeO_6$ were performed at 9.4 and 14.1 T. However, due to the severe acoustic ringing of the probes used at the very low resonance frequency of $^{39}$K, and to the observation of background $^{39}$K resonances, no exploitable data could be obtained even after several days of acquisition.

DIFFax and FAULTS programs[28,29] have been widely used to better understand stacking faults of alkali transition metal oxides.[30–36] In this work, they were used to build up various stacking sequences of $NaKNi_2TeO_6$ with a perfect Na/K alternation, and then stacking faults could be generated by statistical distribution of these stacking configurations. In doing so, X-ray diffraction powder patterns could be simulated and then compared with experimental ones. Practically, sodium and potassium blocks – with a honeycomb Ni/Te slab and an alkali layer above – were created from the structural models of $Na_2Ni_2TeO_6$ and $K_2Ni_2TeO_6$, as well as different stacking vectors to alternately superimpose the blocks (see Supporting Information section for details).

DFT calculations including full structural relaxations were performed for $Na_2Ni_2TeO_6$ with the crystallographic structure provided by Evstigneeva *et al.*[11] as the starting model. Structures were built up with various sodium ion distributions to account for their multiple environments (edge-sharing and/or face-sharing trigonal prisms, Figure S1). Additional structures were then generated with "zigzag" tellurium sequences by substituting one nickel for tellurium cations at $z = 0.5$. In the crystallographic structures of $Na_2Ni_2TeO_6$ and $K_2Ni_2TeO_6$ (Table S1), the alkali positions are the same and the only difference is the occupancy of the three alkali sites. It was thus assumed that no particular alkali/vacancy ordering could be formed and consequently $K_2Ni_2TeO_6$ input structures were obtained by replacing sodium by potassium cations from all the previously generated $Na_2Ni_2TeO_6$ configurations.

Secondly, random *intralayer* alkali distributions were considered for different $Na_{2-x}K_xNi_2TeO_6$ compositions assuming a theoretical solid-solution behavior, *i.e.* sodium to potassium substitution within the same alkali layer, with an equivalent degree of substitution for each layer. To do so, $1\times2\times1$ (236 atoms) and $2\times2\times1$ (472 atoms) supercells were necessary. Lastly, for the particular $NaKNi_2TeO_6$ compositions, the perfect alternation of pure sodium and pure potassium layers was compared to configurations with a progressive random Na/K *interlayer* mixing.

All these crystallographic structures were relaxed using the VASP program package[37] using PAW pseudopotentials[38] for the atomic description and the rotationally invariant DFT+U formalism of Dudarev[39] within the PBE generalized gradient approximation[40] for the exchange and correlation potential and $U_{eff} = 6.2$ eV for Ni. The convergence criteria were set with atomic forces smaller than $2.10^{-3}$ eV/Å$^{-1}$, an energy cut-off of 600 eV for the plane-wave basis set and a k-point grid density for Brillouin zone integration of at least 1000/at. The relative energies of all these structures are given here in meV per $A_2Ni_2TeO_6$.

The Fermi contact shifts were obtained from the computed isotropic hyperfine coupling parameters, as discussed in our previous works.[41–44] The Curie temperature was taken from a previous measurement for $Na_2Ni_2TeO_6$ (34 K)[14] and it was assumed to be the same for all compounds. The theoretical value of molar magnetic susceptibility calculated by Curie's law was used for the Fermi contact shift calculations. The temperature at which the Fermi contact shifts were calculated, was chosen to be 320 K, which is the approximate temperature inside the rotor at a spinning rate of 30 kHz.

**Results**

The synthesis of P2-type $Na_2Ni_2TeO_6$ and $K_2Ni_2TeO_6$ precursors is first verified by laboratory X-ray powder diffraction (Figure S2). For the potassium layered compound, the pattern is in good agreement with the literature[17] and can be indexed with the $P6_3/mcm$ space group, indicating straight chains of tellurium cations. For the sodium analog, with the above-mentioned synthesis conditions the $P6_322$ space group appears more suitable to index the pattern, showing here that the "zigzag" sequence is preferred like in $Na_2Co_2TeO_6$.[13]

Figure 2 gathers the XRPD patterns collected after heating an equimolar mixture of $Na_2Ni_2TeO_6$ and $K_2Ni_2TeO_6$ in different heating conditions. After 9 hours at 200 °C, the main observation is the decrease of the (002) peaks of the layered precursors and the in-between growth of an intense peak at an averaged *d*-space value. As no more trace of the precursors is visible for the syntheses performed at 400 °C and above, the reaction could be considered complete.

Focusing now on the details of the XRPD patterns, the appearance of a superstructure peak at $2\theta = 7$ ° corresponds to a *d*-space value twice larger than the one of the main peak at $2\theta = 15$ °. A doubled periodicity along the $c_{hex.}$-axis is logically suggested, a could be explained by an

alternation of sodium and potassium layers as it has been previously observed in OP4-$Li_xNa_yCoO_2$ phase.[20,45,46] Then it is important to observe the changes in the range 2θ = 18–29 ° with various heating temperatures (inset of Figure 2). Logically, there is a progressive increase in crystallinity with both the temperature and the duration of the heat treatment. Interestingly the relative intensity of the two close peaks around 19.5 ° evolves with the synthesis conditions. With higher temperature and longer heating, the second peak becomes more important. This evolution calls for a change of the stacking sequence of the honeycomb layer by analogy with previous works on P2-type $A_2M_2TeO_6$ compounds[11,14]

Overall, from the XRPD patterns it seems reasonable to assume the formation a new layered compound $NaKNi_2TeO_6$ with alternated sodium and potassium layers. In order to obtain other $Na_{2-x}K_xNi_2TeO_6$ compositions, the initial proportions of the layered precursors have been tuned. However, in all our attempts a biphasic product was finally obtained ($NaKNi_2TeO_6$ and $Na_2Ni_2TeO_6$ or $K_2Ni_2TeO_6$ whether the nominal mixture was sodium-rich or potassium rich, respectively).

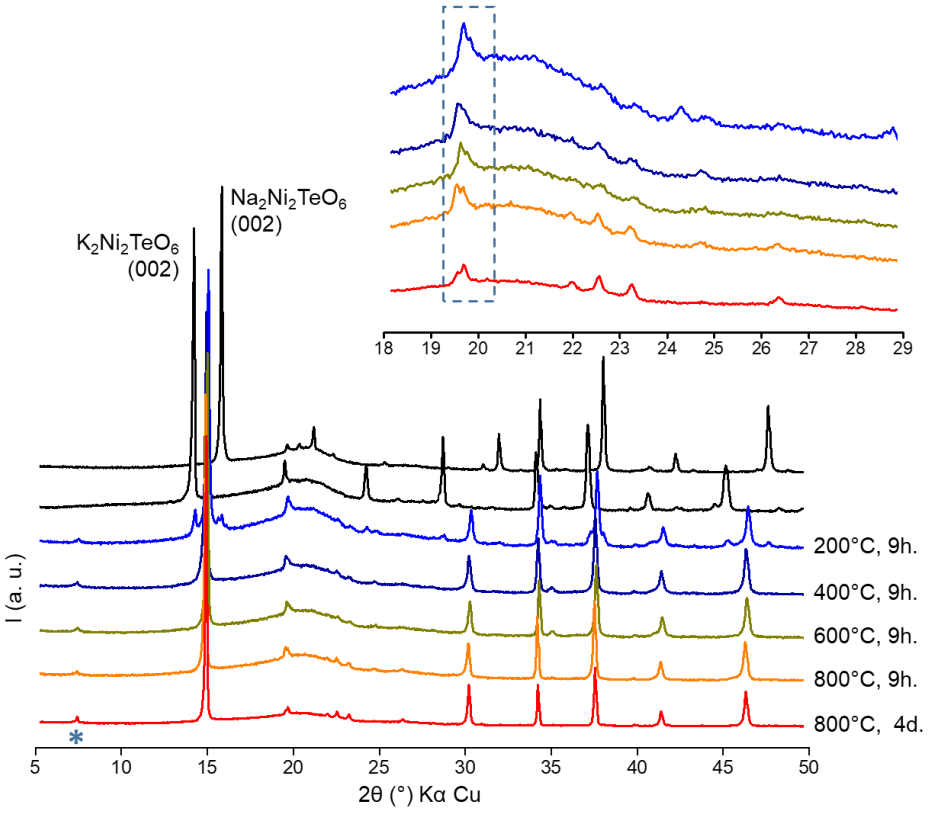

*Figure 2: XRPD patterns of $Na_2Ni_2TeO_6$ and $K_2Ni_2TeO_6$ (black lines) and obtained after heating stoichiometric mixtures in different conditions (colored lines). Intensities are normalized for a better comparison. Symbol (*) indicates the superstructure peak at low angle accounting for the alternation of sodium and potassium blocks. The inset highlights the other superstructure peaks, with a dashed rectangle focusing on the intensity evolution.*

The $NaKNi_2TeO_6$ powder sample obtained after heating 9 hours at 800 °C was analyzed using SXRPD, so to principally enable full structure resolution. The smallest hexagonal cell allowing the indexation of both the main and the superstructure peaks has lattice parameters $a$ = 5.225(1) Å and $c$ = 35.403(1) Å (Figure S3). These lattice parameters correspond to an average of those of $Na_2Ni_2TeO_6$ and $K_2Ni_2TeO_6$, with however a tripled $c_{hex.}$-axis cell parameter (6 layers), likely indicating a complex stacking ordering. However, our attempts to build a complete structural description accounting for all superstructure peaks' intensities were unsuccessful, whatever the space group and atomic distributions we considered. To understand why no meaningful structural model enables a good Rietveld refinement of the SXRPD pattern, electron diffraction was carried out on the same sample (Figure S4). The main spots can be indexed in a hexagonal cell with parameters values $a$ = 5.22 Å and $c$ = 11.8 Å. Additional weak reflections are also observed and need a 2 × $a$ and 3 × $c$ superstructure. The values of $a$ and 3 × $c$ are in line with the SXRPD refinement, but the 2 × $a$ superstructure is not explained and thus confirms the complexity of this crystallographic structure. Note that very recently a similar 2 × $a$ superstructure was also proposed by high-resolution TEM for $Na_2Ni_2TeO_6$.[47]

Additionally, $^{23}$Na solid-state NMR analyses were performed on the $Na_2Ni_2TeO_6$ and $NaKNi_2TeO_6$ in order to get more insight into the local structure of the sodium ions. This technique is extensively being used to investigate alkali transition metal layered oxides and other battery electrode materials, in order to specifically determine the insertion site of the alkali ions during reversible electrochemical cycling.[48,49] As shown in Figure 3, the NMR spectrum of $NaNi_2TeO_6$ shows a major isotropic peak at δ = 677 ppm. Although the sodium ions occupy

different sites (Figure 1c), their high mobility results in an averaged unique peak as it has been already observed in other P2- and P3-type sodium transition metal oxides.[50–53] A unique isotropic signal located at δ = 825 ppm was observed for $NaKNi_2TeO_6$. The presence of a single resonance for $NaKNi_2TeO_6$ confirms that the reaction leading to the alkali-mixed compositions is indeed complete (absence of residual reagent signature at 677 ppm), and that no crystalline or amorphous by-products were formed.

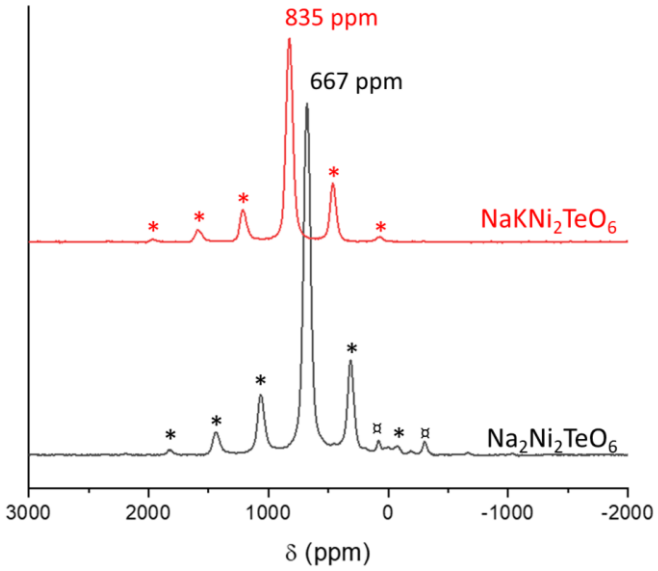


*Figure 3: $^{23}$Na MAS-NMR spectra of $NaKNi_2TeO_6$ (top, in red) and $Na_2Ni_2TeO_6$ (bottom, in black), with spinning sidebands (*). For $Na_2Ni_2TeO_6$, weak signals are also observed in some batches* (¤) *and could be assigned to sodium cations in the honeycomb layer, such as in the layered compound O'3-$Na_3Ni_{1.5}TeO_6$.[54] possible sodium cations present in the honeycomb layer. Spectra are recorded at 7.05 T using a Hahn-Echo sequence synchronized with one rotor rotation period ($\nu_r$ = 30 kHz).*

## Discussion

Heating a mixture of $Na_2Ni_2TeO_6$ and $K_2Ni_2TeO_6$ leads to a new phase $NaKNi_2TeO_6$. Thanks to XRPD, an alternation of sodium and potassium layers is proposed. Very recently the group of Masese investigated the same compound and confirmed the ordering of the alkali layers with high-resolution TEM.[55] The section hereafter aims at going further into the details of this

layered structure by confronting experimental results (powder diffraction and solid-state NMR spectra) with a theoretical approach based on DFT calculations and stacking faults simulations.

First-principles DFT calculations were first performed on the $Na_2Ni_2TeO_6$ and $K_2Ni_2TeO_6$. In both cases, the most stable configurations are obtained when $AO_6$ prisms only share edges with the above and below $NiO_6$ and $TeO_6$ octahedra. Structures with a fraction of prisms sharing faces are systematically less stable, in particular when $TeO_6$ octahedra are facing (Figure S5). Focusing on configurations with $AO_6$ prisms sharing edges only, structures with straight sequences of tellurium are favored with, however, negligible energy stabilization (within the thermal activation energy) compared to the "zigzag" sequences. This suggests no impact of the Ni/Te interlayer sequence on the edge-sharing preference of the $AO_6$ prisms which allows restricting the number of DFT calculations for alkali-mixed compositions to configurations with only edge-sharing $AO_6$ prisms and straight sequences of tellurium cations.

In Figure 4, the formation energy of the relaxed configurations $Na_{2-x}K_xNi_2TeO_6$ ($0 \leq x \leq 2$) is plotted with respect to the proportional mixture of $Na_2Ni_2TeO_6$ and $K_2Ni_2TeO_6$ (considering their most stable configurations). The positive bell-shape curve indicates a significant energy destabilization, even for limited amount of substitution (from either the sodium or the potassium analog). The analysis of the relaxed structures reveals that random $Na^+/K^+$ distributions within the same alkali layer induces significant distortions of the $NaO_6$ octahedra, and to a lower extent the $KO_6$ octahedra, while the local structure of Ni and Te are not altered. Hence, the difference in $Na^+$ and $K^+$ ionic radii induces local mechanical stress which results in a volume expansion of the alkali layer, therefore penalizing the interlayer electrostatic energy (Figure S6). In contrast, structures in which Na and K lie in distinct layers are preferred and any mixing leads to a loss of electrostatic interactions (Figure S7). This interpretation agrees with the similar line width of the NMR spectra of both $Na_2Ni_2TeO_6$ and $NaKNi_2TeO_6$. Indeed, the hypothesis of simultaneous occupation of both sodium and potassium cations in the same layer would have

induced more local distortions and sodium environment distributions and consequently a larger width, as observed for O3-type $Li_{3-x}Na_xNi_2SbO_6$ solid-solution.[56]

Interestingly, no quenching at the end of the thermal treatment is necessary to avoid phase segregation in contrast to what is observed for the alkali-ordered OP4-$Li_xNa_yCoO_2$ under slow cooling procedure.[46], $NaKNi_2TeO_6$ can therefore be considered as thermodynamically stable with respect to segregation. This experimental fact is consistent with the phase stability diagram of Figure 4 showing that structures with alternating Na and K layers lie only ~10meV/f.u. above the segregation reference. Although positive, such a small formation energy can easily switch to negative values once entropy contributions are considered. Indeed, configuration entropy is expected to be larger in alkali-mixed compositions (Na/K) than single-alkali compositions (Na or K), therefore stabilizing the former over the latter. It is also important to remind here that different occupancies of the three available alkali cations sites are reported from the structural description of $Na_2Ni_2TeO_6$ and $K_2Ni_2TeO_6$ (Table S1). As the heat treatment leading to the mixed $NaKNi_2TeO_6$ could be seen as a second sintering of the precursors, it is reasonable to assume a higher fraction of alkali ions in the most stable sites (edge-sharing prisms) in $NaKNi_2TeO_6$ compared to the $Na_2Ni_2TeO_6$ and $K_2Ni_2TeO_6$ precursors Accordingly, the $Na_2Ni_2TeO_6$ and $K_2Ni_2TeO_6$ edge-sharing configurations taken as references in the phase stability diagram are artificially stabilized with respect to mixed edge-face-sharing configurations, as corroborated by our DFT calculations (see Figure S5). Raising up the reference energy of the phase stability diagram of Figure 4 by considering configurations with fraction of face sharing alkali sites should therefore contribute to stabilizing the alkali-mixed $NaKNi_2TeO_6$ phase with respect to segregation.

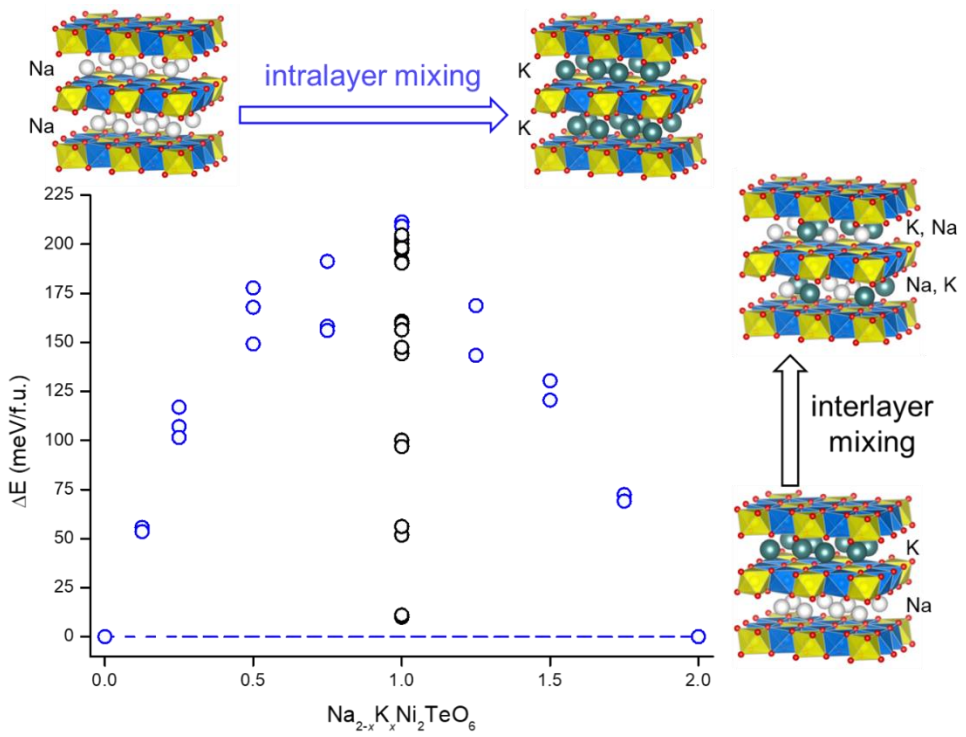


*Figure 4:Phase stability diagram of the $Na_{2-x}K_xNi_2TeO_6$ system with respect to the proportional mixture of $Na_2Ni_2TeO6$ and $K_2Ni_2TeO_6$ (dash blue line), as obtained from DFT+U calculations and showing a significant energy destabilization for random distributions of sodium and potassium within the same alkali layer, either assuming a solid-solution behavior $Na_{2-x}K_xNi_2TeO_6$ with progressive Na/K intralayer mixing (blue circles) or focusing on a fixed $NaKNi_2TeO_6$ composition with a progressive Na/K interlayer mixing (black circles). Only configurations with edge-sharing $AO_6$ prisms are considered for all the structure relaxation.*

Once the alternation of sodium and potassium layers is validated, the next question lies on the thicknesses of these layers in $NaKNi_2TeO_6$. In the work of Masese *et al.*, the alkali layers thickness in $NaKNi_2TeO_6$ is found similar to those in $Na_2Ni_2TeO_6$ and $K_2Ni_2TeO_6$.[55] Such observation appears not in line with the $^{23}$Na NMR in Figure 3, for which a shift of the major isotropic peak is observed (from 667 to 835 ppm). To better understand this significant difference, theoretical NMR shifts were calculated for particular configurations after DFT structural relaxations (Tables S2 and S3). For $Na_2Ni_2TeO_6$ a higher NMR shift is observed when $NaO_6$ prisms share only edges with $NiO_6$ and $TeO_6$ octahedra. The stacking sequence, *i.e.* the relative position of tellurium cations along the $c_{hex.}$-axis, plays a secondary role and the "zigzag" configuration also shifts the NMR peaks to higher values. Regarding $NaKNi_2TeO_6$, it

appears that the introduction of potassium layers does not significantly affect the local environment of the sodium ions, as similar simulated peak shift values are obtained for both compounds. In DFT calculations, logically thicker alkali layers are observed for configurations with more face-sharing sites (Figure S8). Keeping in mind the strong ionic mobility which averages the experimental NMR shift and following our above hypothesis regarding the relative stability of $NaKNi_2TeO_6$, the higher peak shift in $NaKNi_2TeO_6$ could be related to a higher proportion of edge-sharing $NaO_6$ prisms than in $Na_2Ni_2TeO_6$.

Although the above sections clearly help to better picture the structure of $NaKNi_2TeO_6$, the analysis of the diffraction patterns is still challenging. In the aperiodic arrangement proposed from high-resolution TEM, honeycomb layers are perfectly superimposed or glided in random directions through each potassium or sodium layers, respectively.[55] As shown in Figure S5, energy differences between $Na_2Ni_2TeO_6$ with straight and "zigzag" sequences of tellurium falls within the thermal activation energy. It is the same for $K_2Ni_2TeO_6$, and therefore it is reasonable to assume that both stacking sequences are actually possible for $NaKNi_2TeO_6$. It is thus necessary to evaluate the influence of the successive position of Ni/Te honeycomb layers in $NaKNi_2TeO_6$ on the diffraction patterns. To do so, we carried out the simulation of the $NaKNi_2TeO_6$ structure using the FAULTS program to evaluate how different stacking configurations could affect the XRPD patterns. Two building blocks were generated with either a sodium or a potassium layer on top of a Ni/Te honeycomb sheet (Figure S9), while different vectors and stacking probabilities were used to simulate patterns with different gliding in their stacking sequences (Figure S10). Owing to the 6-fold symmetry of the honeycomb layer, five distinct stacking models are possible, with or without gliding through sodium and/or potassium layers (Figure S11). The corresponding simulated XRPD patterns are shown in Figures S12 to S16, without or with 10 % of stacking faults. Comparing to experimental XRPD patterns, the

combination of two stacking models is the only way to fully assign each peak, especially the two just around 19.5 ° (Figure 5). The first model exhibits a straight stacking, for both the potassium and the sodium layers, with a 10 % of faults for the sodium layer (Figure S12). The second is characterized by a straight sequence through the potassium layer and a "zigzag" one through the sodium layers (Figures S14). Interestingly, no model with block gliding through potassium layers is required, in agreement with the aperiodic stacking already reported.[55] It is also in line with the different stacking sequences observed for $Na_2Ni_2TeO_6$ and $K_2Ni_2TeO_6$ synthesized at 800 °C (Figure S2).

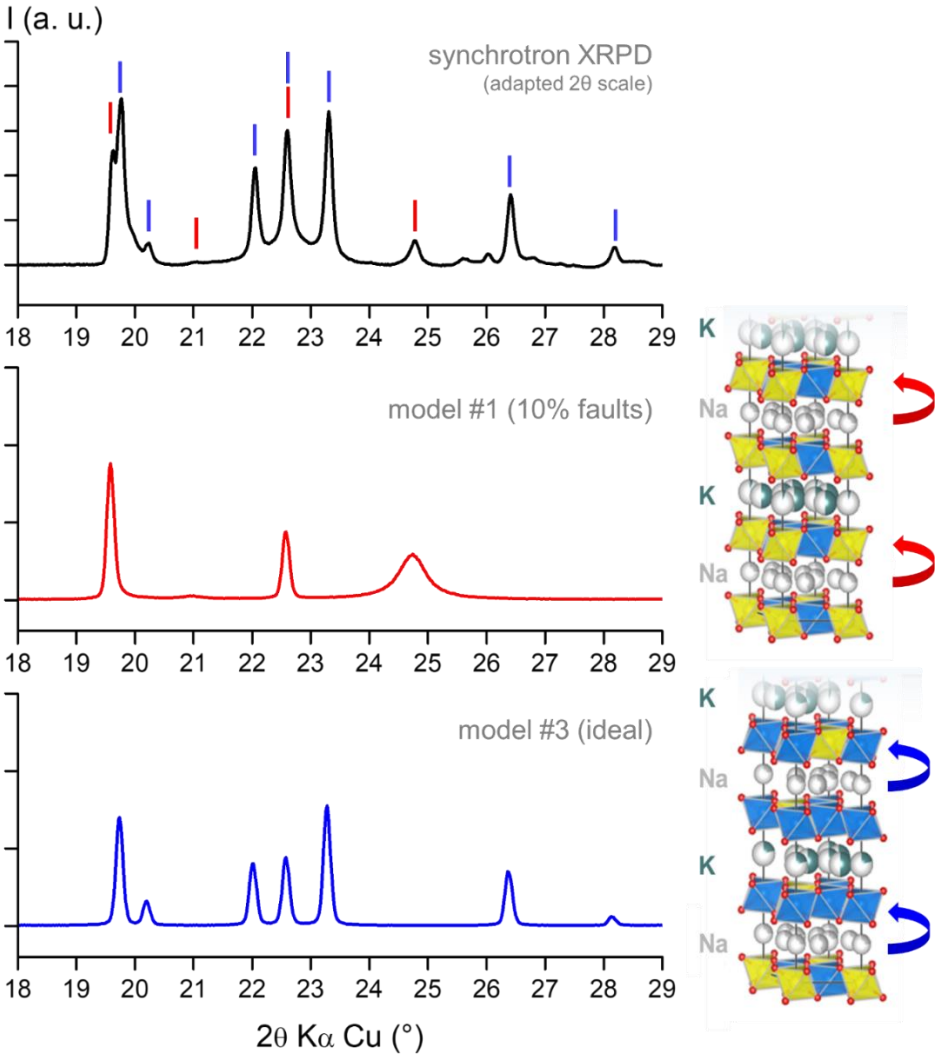


*Figure 5: Comparison between experimental SXRPD pattern and the simulated ones for stacking models #1 with 10% of stacking faults (blue line) and #3 without faults(red line). The vertical bars on the top panel highlight the peaks assigned to one model or the other. The ideal*

*models are provided on the right, with arrows showing the stacking with or without gliding (blue and red, respectively).*

After the crystallographic structure, the discussion also needs to focus on the formation of $NaKNi_2TeO_6$. From the Figure 2, solid-solid reaction between $Na_2Ni_2TeO_6$ and $K_2Ni_2TeO_6$ precursors occurs at very moderate temperatures. This in sharp contrast with other alkali-mixed compositions. Indeed, OP4-$Li_xNa_yCoO_2$ is formed above 800 °C from a mixture of O3-$LiCoO_2$ and P2-$Na_xCoO_2$,[46] and that a similarly elevated temperature range is needed to obtain O3-$Li_{3-x}Na_xNi_2SbO_6$.[56] P2-type $A_2M_2TeO_6$ oxides have been recently investigated for their high ionic conductivities, around 4-11 S/m at 300 °C,[11,17] thanks to the high mobility of the alkali ions within the alkali layers. This certainly plays a key role in the formation of $NaKNi_2TeO_6$ and strongly suggests a topotactic and simultaneous $Na^+/K^+$ and $K^+/Na^+$ ionic exchanges within the alkali layers, although such mixed-alkali occupancy is considered unstable by DFT calculations.

## Conclusion

Alkali-mixed layered oxide $NaKNi_2TeO_6$ could be obtained by solid-solid reaction between analogs $Na_2Ni_2TeO_6$ and $K_2Ni_2TeO_6$. From the structural point of view, the alternation of sodium and potassium layers along the $c_{hex.}$-axis is validated through the combination of XRD, solid-state NMR and DFT calculations. Thanks to stacking faults simulations, it seems clear that multiple stacking sequences occur simultaneously in $NaKNi_2TeO_6$.

The fact that the experimental patterns result as a combination of both structural models indicates that the areas exhibiting different stacking sequences cover a significant length scale. They could be present in different crystallites, or as intergrowth within the same crystallites. Their relative amounts evolves with the synthesis conditions (temperature and duration).

Obtaining single crystals could be a solution to get a fine crystallographic description and to eventually validate the hypothesis of a higher fraction of edge-sharing alkali sites in $NaKNi_2TeO_6$ proposed by both DFT calculations and solid-state NMR. Contrary to the OP4-$Li_xNa_yCoO_2$ phase, here it seems achievable as slow cooling allows the formation of $NaKNi_2TeO_6$.

The application of $NaKNi_2TeO_6$ as electrode material with liquid NaK negative electrode has been recently proposed.[55] However, the presence of tellurium cations significantly limits the specific capacity. The family of alkali transition metal compounds is already important, but the report of $NaKNi_2TeO_6$ confirms that new compositions with alkali mixing and/or ordering could be still discovered, with eventually promising physical features and interesting applications.

**Acknowledgement**

Matthieu Saubanère (ICGM) is acknowledged for fruitful discussion. Paula Sanz-Camacho (ICMCB) is acknowledged for technical support with the $^{23}Na$ NMR acquisitions. BL04-MSPD staff of CELLS-ALBA synchrotron is acknowledged for granting beamtime through InHouse quota (proposal 2020014011)

**Supporting information**

Crystallographic features and XRPD patterns of $Na_2Ni_2TeO_6$ and $K_2Ni_2TeO_6$, SXRPD pattern and TEM image of $NaKNi_2TeO_6$, additional observations from the DFT calculations, general methodology for the stacking faults simulation in $NaKNi_2TeO_6$.

## References


(1) Abakumov, A. M.; Fedotov, S. S.; Antipov, E. V; Tarascon, J.-M. Solid State Chemistry for Developing Better Metal-Ion Batteries. *Nat. Commun.* **2020**, *11* (1), 4976. https://doi.org/10.1038/s41467-020-18736-7.

(2) Kubota, K.; Kumakura, S.; Yoda, Y.; Kuroki, K.; Komaba, S. Electrochemistry and Solid-State Chemistry of $NaMeO_2$ (Me = 3d Transition Metals). *Adv. Energy Mater.* **2018**, *8* (17), 1703415. https://doi.org/https://doi.org/10.1002/aenm.201703415.

(3) Delmas, C.; Carlier, D.; Guignard, M. The Layered Oxides in Lithium and Sodium-Ion Batteries: A Solid-State Chemistry Approach. *Adv. Energy Mater.* **2021**, *11* (2), 2001201. https://doi.org/https://doi.org/10.1002/aenm.202001201.

(4) Sathiya, M.; Rousse, G.; Ramesha, K.; Laisa, C. P.; Vezin, H.; Sougrati, M. T.; Doublet, M.; Foix, D.; Gonbeau, D.; Walker, W.; et al. Reversible Anionic Redox Chemistry in High-Capacity Layered-Oxide Electrodes. *Nat. Mater.* **2013**, *12* (9), 827–835. https://doi.org/10.1038/nmat3699.

(5) Sathiya, M.; Ramesha, K.; Rousse, G.; Foix, D.; Gonbeau, D.; Prakash, A. S.; Doublet, M. L.; Hemalatha, K. High Performance $Li_2Ru_{1-y}Mn_yO_3$ ($0.2 \leq y \leq 0.8$) Cathode Materials for Rechargeable Lithium-Ion Batteries: Their Understanding. *Chem. Mater.* **2013**, *25*, 1121--1131. https://doi.org/10.1021/cm400193m.

(6) Saubanère, M.; Ben Yahia, M.; Lebègue, S.; Doublet, M. L. An Intuitive and Efficient Method for Cell Voltage Prediction of Lithium and Sodium-Ion Batteries. *Nature Commun.* **2104**, *5*, 5559. https://doi.org/10.1038/ncomms6559.

(7) McCalla, E.; Abakumov, A. M.; Saubanère, M.; Foix, D.; Berg, E. J.; Rousse, G.; Doublet, M.-L.; Gonbeau, D.; Novák, P.; Van Tendeloo, G.; et al. Visualization of O-O Peroxo-like Dimers in High-Capacity Layered Oxides for Li-Ion Batteries. *Science.* **2015**, *350* (6267), 1516–1521. https://doi.org/10.1126/science.aac8260.

(8) Pearce, P. E.; Perez, A. J.; Rousse, G.; Saubanere, M.; Batuk, D.; Foix, D.; McCalla, E.; Abakumov, A. M.; Van Tendeloo, G.; Doublet, M.-L.; et al. Evidence for Anionic Redox Activity in a Tridimensional-Ordered Li-Rich Positive Electrode β-$Li_2IrO_3$. *Nat Mater* **2017**, *16*, 580–586. https://doi.org/doi.org/10.1038/nmat4864.

(9) Yahia, M. Ben; Vergnet, J.; Saubanère, M.; Doublet, M.-L. Unified Picture of Anionic Redox in Li/Na-Ion Batteries. *Nat. Mater.* **2019**, *18*, 496--502. https://doi.org/10.1038/s41563-019-0318-3.

(10) Kanyolo, G. M.; Masese, T.; Matsubara, N.; Chen, C.-Y.; Rizell, J.; Huang, Z.-D.; Sassa, Y.; Månsson, M.; Senoh, H.; Matsumoto, H. Honeycomb Layered Oxides: Structure, Energy Storage, Transport, Topology and Relevant Insights. *Chem. Soc. Rev.* **2021**, *50* (6), 3990–4030. https://doi.org/10.1039/D0CS00320D.

(11) Evstigneeva, M. A.; Nalbandyan, V. B.; Petrenko, A. A.; Medvedev, B. S.; Kataev, A. A. A New Family of Fast Sodium Ion Conductors: $Na_2M_2TeO_6$ (M = Ni, Co, Zn, Mg). *Chem. Mater.* **2011**, *23* (5), 1174–1181. https://doi.org/10.1021/cm102629g.

(12) Delmas, C.; Fouassier, C.; Hagenmuller, P. Structural Classification and Properties of the Layered Oxides. *Phys. B+C* **1980**, *99* (1–4), 81–85. https://doi.org/10.1016/0378-4363(80)90214-4.

(13) Viciu, L.; Huang, Q.; Morosan, E.; Zandbergen, H. W.; Greenbaum, N. I.; McQueen, T.; Cava, R. J. Structure and Basic Magnetic Properties of the Honeycomb Lattice Compounds $Na_2Co_2TeO_6$ and $Na_3Co_2SbO_6$. *J. Solid State Chem.* **2007**, *180* (3), 1060–1067. https://doi.org/10.1016/j.jssc.2007.01.002.

(14) Berthelot, R.; Schmidt, W.; Sleight, A. W.; Subramanian, M. A. Studies on Solid Solutions Based on Layered Honeycomb-Ordered Phases P2-$Na_2M_2TeO_6$ (M=Co, Ni, Zn). *J. Solid State Chem.* **2012**, *196*, 225–231. https://doi.org/10.1016/j.jssc.2012.06.022.

(15) Gupta, A.; Buddie Mullins, C.; Goodenough, J. B. $Na_2Ni_2TeO_6$: Evaluation as a Cathode for Sodium Battery. *J. Power Sources* **2013**, *243*, 817–821. https://doi.org/10.1016/j.jpowsour.2013.06.073.

(16) Bera, A. K.; Yusuf, S. M. Temperature-Dependent Na-Ion Conduction and Its Pathways in the Crystal Structure of the Layered Battery Material $Na_2Ni_2TeO_6$. *J. Phys. Chem. C* **2020**, *124* (8), 4421–4429. https://doi.org/10.1021/acs.jpcc.9b11191.

(17) Masese, T.; Yoshii, K.; Yamaguchi, Y.; Okumura, T.; Huang, Z. D.; Kato, M.; Kubota, K.; Furutani, J.; Orikasa, Y.; Senoh, H.; et al. Rechargeable Potassium-Ion Batteries with Honeycomb-Layered Tellurates as High Voltage Cathodes and Fast Potassium-Ion Conductors. *Nat. Commun.* **2018**, *9*, 3823. https://doi.org/10.1038/s41467-018-06343-6.

(18) Masese, T.; Yoshii, K.; Kato, M.; Kubota, K.; Huang, Z. D.; Senoh, H.; Shikano, M. A High Voltage Honeycomb Layered Cathode Framework for Rechargeable Potassium-Ion Battery: P2-Type $K_{2/3}Ni_{1/3}Co_{1/3}Te_{1/3}O_2$. *Chem. Commun.* **2019**, *55* (7), 985–988. https://doi.org/10.1039/c8cc07239f.

(19) Masese, T.; Miyazaki, Y.; Mbiti Kanyolo, G.; Takahashi, T.; Ito, M.; Senoh, H.; Saito, T. Topological Defects and Unique Stacking Disorders in Honeycomb Layered Oxide $K_2Ni_2TeO_6$ Nanomaterials: Implications for Rechargeable Batteries. *ACS Appl. Nano Mater.* **2021**, *4* (1), 279–287. https://doi.org/10.1021/acsanm.0c02601.

(20) Balsys, R. J.; Lindsay Davis, R. The Structure of $Li_{0.43}Na_{0.36}CoO_{1.96}$ Using Neutron Powder Diffraction. *Solid State Ionics* **1994**, *69* (1), 69–74. https://doi.org/https://doi.org/10.1016/0167-2738(94)90451-0.

(21) Komaba, S.; Yabuuchi, N.; Kawamoto, Y. A New Polymorph of Layered $LiCoO_2$. *Chem. Lett.* **2009**, *38(10)*, 954. https://doi.org/10.1246/cl.2009.954.

(22) Berthelot, R.; Carlier, D.; Pollet, M.; Doumerc, J.-P.; Delmas, C. Synthesis and Investigations on an O4-$LiCoO_2$ Polytype. *Electrochem. Solid-State Lett.* **2009**, *12* (11), A207–A210. https://doi.org/10.1149/1.3204643.

(23) Yabuuchi, N.; Kawamoto, Y.; Hara, R.; Ishigaki, T.; Hoshikawa, A.; Yonemura, M.; Kamiyama, T.; Komaba, S. A Comparative Study of $LiCoO_2$ Polymorphs: Structural and Electrochemical Characterization of O2-, O3-, and O4-Type Phases. *Inorg. Chem.* **2013**, *52* (15), 9131–9142. https://doi.org/10.1021/ic4013922.

(24) Nalbandyan, V. B.; Petrenko, A. A.; Evstigneeva, M. A. Heterovalent Substitutions in $Na_2M_2TeO_6$ Family: Crystal Structure, Fast Sodium Ion Conduction and Phase Transition of $Na_2LiFeTeO_6$. *Solid State Ionics* **2013**, *233*, 7–11. https://doi.org/10.1016/j.ssi.2012.12.002.

(25) Fauth, F.; Peral, I.; Popescu, C.; Knapp, M. The New Material Science Powder Diffraction Beamline at ALBA Synchrotron. *Powder Diffr.* **2013**, *28* (S2), S360–S370. https://doi.org/10.1017/S0885715613000900.

(26) Fauth, F.; Boer, R.; Gil-Ortiz, F.; Popescu, C.; Vallcorba, O.; Peral, I.; Fullà, D.; Benach, J.; Juanhuix, J. The Crystallography Stations at the Alba Synchrotron. *Eur. Phys. J. Plus* **2015**, *130* (8), 160. https://doi.org/10.1140/epjp/i2015-15160-y.

(27) Rodríguez-Carvajal, J. Recent Advances in Magnetic Structure Determination by Neutron Powder Diffraction. *Phys. B Condens. Matter* **1993**, *192* (1), 55–69. https://doi.org/https://doi.org/10.1016/0921-4526(93)90108-I.

(28) Treacy, M. M. J.; Newsam, J. M.; Deem, M. W. A General Recursion Method for Calculating Diffracted Intensities from Crystals Containing Planar Faults. *Proc. Math. Phys. Sci.* **1991**, *433* (1889), 499–520. https://doi.org/10.1098/rspa.1991.0062.

(29) Casas-Cabanas, M.; Reynaud, M.; Rikarte, J.; Horbach, P.; Rodriguez-Carvajal, J. FAULTS: A Program for Refinement of Structures with Extended Defects. *J. Appl. Crystallogr.* **2016**, *49* (6), 2259–2269. https://doi.org/10.1107/S1600576716014473.

(30) Casas-Cabanas, M.; Rodríguez-Carvajal, J.; Canales-Vázquez, J.; Laligant, Y.; Lacorre, P.; Palacín, M. R. Microstructural Characterisation of Battery Materials Using Powder Diffraction Data: DIFFaX, FAULTS and SH-FullProf Approaches. *J. Power Sources* **2007**, *174* (2), 414–420. https://doi.org/10.1016/j.jpowsour.2007.06.216.

(31) Boulineau, A.; Croguennec, L.; Delmas, C.; Weill, F. Structure of $Li_2MnO_3$ with Different Degrees of Defects. *Solid State Ionics* **2010**, *180* (40), 1652–1659. https://doi.org/10.1016/j.ssi.2009.10.020.

(32) Boulineau, A.; Croguennec, L.; Delmas, C.; Weill, F. Thermal Stability of $Li_2MnO_3$: From Localized Defects to the Spinel Phase. *Dalt. Trans.* **2012**, *41* (5), 1574–1581. https://doi.org/10.1039/c1dt11598g.

(33) Serrano-Sevillano, J.; Reynaud, M.; Saracibar, A.; Altantzis, T.; Bals, S.; van Tendeloo, G.; Casas-Cabanas, M. Enhanced Electrochemical Performance of Li-Rich Cathode Materials through Microstructural Control. *Phys. Chem. Chem. Phys.* **2018**, *20* (35), 23112–23122. https://doi.org/10.1039/C8CP04181D.

(34) Bianchini, M.; Schiele, A.; Schweidler, S.; Sicolo, S.; Fauth, F.; Suard, E.; Indris, S.; Mazilkin, A.; Nagel, P.; Schuppler, S.; et al. From $LiNiO_2$ to $Li_2NiO_3$: Synthesis, Structures and Electrochemical Mechanisms in Li-Rich Nickel Oxides. *Chem. Mater.* **2020**, *32* (21), 9211–9227. https://doi.org/10.1021/acs.chemmater.0c02880.

(35) Shunmugasundaram, R.; Arumugam, R. S.; Dahn, J. R. A Study of Stacking Faults and Superlattice Ordering in Some Li-Rich Layered Transition Metal Oxide Positive Electrode Materials. *J. Electrochem. Soc.* **2016**, *163* (7), A1394–A1400. https://doi.org/10.1149/2.1221607jes.

(36) Mortemard de Boisse, B.; Reynaud, M.; Ma, J.; Kikkawa, J.; Nishimura, S.; Casas-Cabanas, M.; Delmas, C.; Okubo, M.; Yamada, A. Coulombic Self-Ordering upon Charging a Large-Capacity Layered Cathode Material for Rechargeable Batteries. *Nat. Commun.* **2019**, *10* (1), 2185. https://doi.org/10.1038/s41467-019-09409-1.

(37) Kresse, G.; Furthmuller, J. Efficiency of Ab-Initio Total Energy Calculations for Metals and Semiconductors Using a Plane-Wave Basis Set. *Comput. Mater. Sci.* **1996**, *6* (1), 15–50.

(38) G.Kresse, D. J. From Ultrasoft Pseudopotentials to the Projector Augmented-Wave Method. *Phys. Rev. B* **1999**, *59* (3), 1758–1775. https://doi.org/10.1103/PhysRevB.59.1758.

(39) Dudarev, S. L.; Botton, G. A.; Savrasov, S. Y.; Humphreys, C. J.; Sutton, A. P. Electron-Energy-Loss Spectra and the Structural Stability of Nickel Oxide: An LSDA+U Study. *Phys. Rev. B* **1998**, *57* (3), 1505–1509. https://doi.org/10.1103/PhysRevB.57.1505.

(40) Perdew, J. P.; Burke, K.; Ernzerhof, M. Generalized Gradient Approximation Made Simple. *Phys. Rev. Lett.* **1996**, *77* (18), 3865–3868. https://doi.org/10.1103/PhysRevLett.77.3865.

(41) Castets, A.; Carlier, D.; Zhang, Y.; Boucher, F.; Marx, N.; Croguennec, L.; Ménétrier, M. Multinuclear NMR and DFT Calculations on the $LiFePO_4.OH$ and $FePO_4.H_2O$ Homeotypic Phases. *J. Phys. Chem. C* **2011**, *115* (32), 16234–16241. https://doi.org/10.1021/jp204767c.

(42) Nguyen, L. H. B.; Sanz Camacho, P.; Broux, T.; Olchowka, J.; Masquelier, C.; Croguennec, L.; Carlier, D. Density Functional Theory-Assisted $^{31}P$ and $^{23}Na$ Magic-Angle Spinning Nuclear Magnetic Resonance Study of the $Na_3V_2(PO_4)_2F_3$–$Na_3V_2(PO_4)_2FO_2$ Solid Solution: Unraveling Its Local and Electronic Structures. *Chem. Mater.* **2019**, *31* (23), 9759–9768. https://doi.org/10.1021/acs.chemmater.9b03546.

(43) Serrano-Sevillano, J.; Carlier, D.; Saracibar, A.; Lopez Del Amo, J. M.; Casas-Cabanas, M. DFT-Assisted Solid-State NMR Characterization of Defects in $Li_2MnO_3$. *Inorg. Chem.* **2019**, *58* (13), 8347–8356. https://doi.org/10.1021/acs.inorgchem.9b00394.

(44) Bamine, T.; Boivin, E.; Boucher, F.; Messinger, R. J.; Salager, E.; Deschamps, M.; Masquelier, C.; Croguennec, L.; Ménétrier, M.; Carlier, D. Understanding Local Defects in Li-Ion Battery Electrodes through Combined DFT/NMR Studies: Application to $LiVPO_4F$. *J. Phys. Chem. C* **2017**, *121* (6), 3219–3227. https://doi.org/10.1021/acs.jpcc.6b11747.

(45) Ren, Z.; Shen, J.; Jiang, S.; Chen, X.; Feng, C.; Xu, Z.; Cao, G. Enhanced Thermopower in an Intergrowth Cobalt Oxide Li 0.48Na0.35CoO2. *J. Phys. Condens. Matter* **2006**, *18* (29), L379.

(46) Berthelot, R.; Pollet, M.; Carlier, D.; Delmas, C. Reinvestigation of the OP4-$(Li/Na)CoO_2$-Layered System and First Evidence of the $(Li/Na/Na)CoO_2$ Phase with OPP9 Oxygen Stacking. *Inorg. Chem.* **2011**, *50* (6), 2420–2430. https://doi.org/10.1021/ic102218w.

(47) Masese, T.; Miyazaki, Y.; Rizell, J.; Kanyolo, G. M.; Takahashi, T.; Ito, M.; Senoh, H.; Saito, T. Unveiling Structural Disorders in Honeycomb Layered Oxide: $Na_2Ni_2TeO_6$. *Materialia* **2021**, *15*, 101003. https://doi.org/https://doi.org/10.1016/j.mtla.2021.101003.

(48) Grey, C. P.; Lee, Y. J. Lithium MAS NMR Studies of Cathode Materials for Lithium-Ion Batteries. *Solid State Sci.* **2003**, *5* (6), 883–894. https://doi.org/10.1016/S1293-2558(03)00113-4.

(49) Pecher, O.; Carretero-Gonzalez, J.; Griffith, K. J.; Grey, C. P. Materials' Methods: NMR in Battery Research. *Chem. Mater.* **2017**, *29* (1), 213–242. https://doi.org/10.1021/acs.chemmater.6b03183.

(50) Kalapsazova, M.; Ivanova, S.; Kukeva, R.; Simova, S.; Wegner, S.; Zhecheva, E.; Stoyanova, R. Combined Use of EPR and $^{23}$Na MAS NMR Spectroscopy for Assessing the Properties of the Mixed Cobalt-Nickel-Manganese Layers of: P3-$Na_yCo_{1-2x}Ni_xMn_xO_2$. *Phys. Chem. Chem. Phys.* **2017**, *19* (39), 27065–27073. https://doi.org/10.1039/c7cp04849a.

(51) Carlier, D.; Blangero, M.; Ménétrier, M.; Pollet, M.; Doumerc, J.-P.; Delmas, C. Sodium Ion Mobility in $Na_xCoO_2$ ($0.6 < x < 0.75$) Cobaltites Studied by 23Na MAS NMR. *Inorg. Chem.* **2009**, *48* (15), 7018–7025. https://doi.org/10.1021/ic900026c.

(52) Carlier, D.; Cheng, J. H.; Berthelot, R.; Guignard, M.; Yoncheva, M.; Stoyanova, R.; Hwang, B. J.; Delmas, C. The P2-$Na_{2/3}Co_{2/3}Mn_{1/3}O_2$ phase: Structure, Physical Properties and Electrochemical Behavior as Positive Electrode in Sodium Battery. *Dalt. Trans.* **2011**, *40* (36), 9306–9312. https://doi.org/10.1039/c1dt10798d.

(53) Blangero, M.; Carlier, D.; Pollet, M.; Darriet, J.; Delmas, C.; Doumerc, J.-P. High-Temperature Phase Transition in the Three-Layered Sodium Cobaltite P'3-$Na_xCoO_2$ ($x\sim0.62$). *Phys. Rev. B Condens. Matter Mater. Phys.* **2008**, *77* (18), 184116.

(54) Grundish, N. S.; Seymour, I. D.; Li, Y.; Sand, J.-B.; Henkelman, G.; Delmas, C.; Goodenough, J. B. Structural and Electrochemical Consequences of Sodium in the Transition-Metal Layer of O′3-$Na_3Ni_{1.5}TeO_6$. *Chem. Mater.* **2020**, *32* (23), 10035–10044. https://doi.org/10.1021/acs.chemmater.0c03248.

(55) Masese, T.; Miyazaki, Y.; Rizell, J.; Kanyolo, G. M.; Chen, C.-Y.; Ubukata, H.; Kubota, K.; Sau, K.; Ikeshoji, T.; Huang, Z.-D.; et al. Mixed Alkali-Ion Transport and Storage in Atomic-Disordered Honeycomb Layered $NaKNi_2TeO_6$. *Nat. Commun.* **2021**, *12* (1), 4660. https://doi.org/10.1038/s41467-021-24694-5.

(56) Vallée, C.; Saubanère, M.; Sanz-Camacho, P.; Biecher, Y.; Fraisse, B.; Suard, E.; Rousse, G.; Carlier, D.; Berthelot, R. Alkali-Glass Behavior in Honeycomb-Type Layered $Li_{3-x}Na_xNi_2SbO_6$ Solid Solution. *Inorg. Chem.* **2019**, *58*, 11546--11552. https://doi.org/10.1021/acs.inorgchem.9b01385.

## TOC graphics

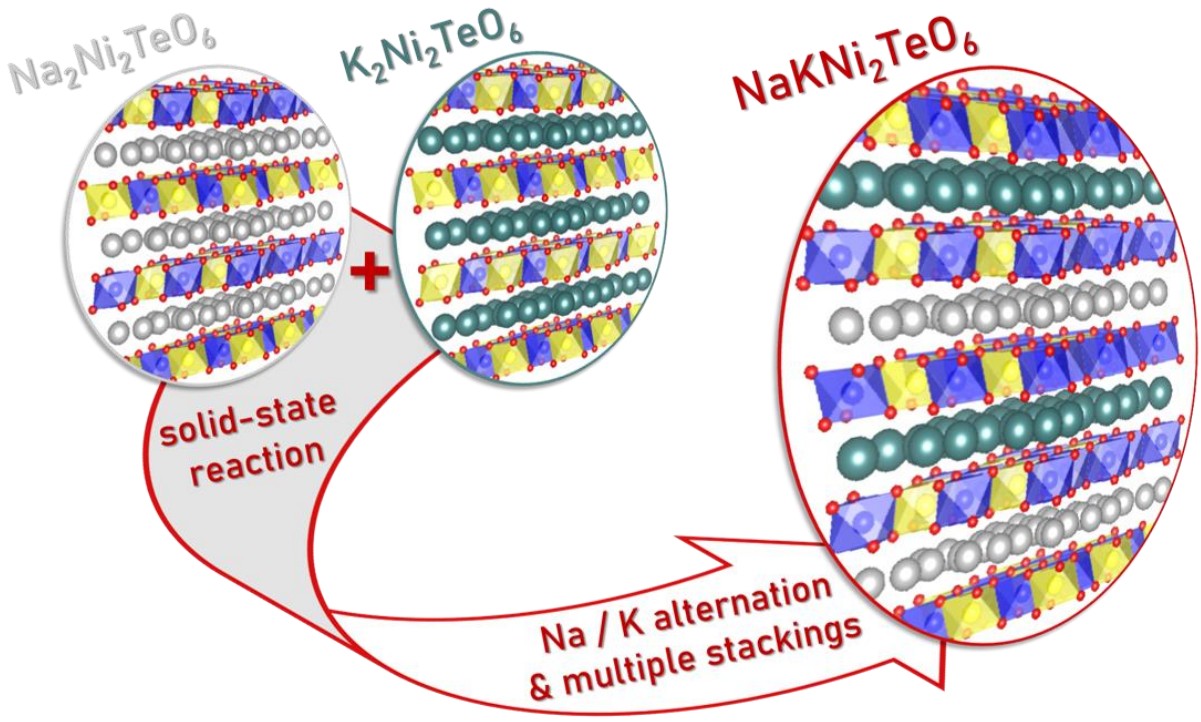


**TOC Synopsis**

Layered oxide $NaKNi_2TeO_6$ is obtained from a stoichiometric mixture of honeycomb layered precursors $Na_2Ni_2TeO_6$ and $K_2Ni_2TeO_6$ and characterized by X-ray diffraction and solid-state NMR. The structure of $NaKNi_2TeO_6$ exhibits an alternation of sodium and potassium layers, and DFT calculations rationalize the existence of this cationic ordering versus phase segregation. An aperiodic stacking prevents from a detailed crystallographic description, but stacking faults simulations reveal multiple possible stacking sequences in the powder material.